Chapter 2

Canopy-scale model

2.1 Theory

2.1.1 Lagrangian dispersal theory

The application of Lagrangian analysis to scalar dispersion within plant canopies was developed by Raupach (1987; 1989a; 1989b) as the so-called localised near-field theory. The theory distinguishes between two regimes of dispersion: the near field and the far field. Dispersion in the near field is dominated by the persistence of the turbulent eddies, and a scalar cloud grows linearly with time in this region as particles tend to maintain their initial speed and direction. In contrast, dispersion in the far field behaves as a random walk that is well described by gradient-diffusion theory. Here the dispersal cloud grows with the square root of time in homogeneous turbulence. Neglect of the near field source contribution should therefore tend to underestimate the scalar concentration, or in the inverse mode, the source strength will be significantly overestimated (as was found, for example, by Katul *et al.* 1997 in their model comparison). Raupach's approach, used here, neglects non-Gaussian properties of the turbulence and relies on the assumptions that (i) the turbulence is locally homogeneous (that is, the near-field contribution can be determined as if the turbulence were homogeneous); and (ii) that dispersion in the far field obeys gradient-diffusion theory. These assumptions are presently thought to be adequate for turbulence regimes typical of plant canopies. Random-flight approaches to Lagrangian

turbulent transfer can allow for non-Gaussian velocity distributions and strong inhomogeneity (Thomson, 1987) but they suffer from significant complexity, high computational demand, noise susceptibility and uncertainty about the governing stochastic equations. Higher-order closure models in an Eulerian or hybrid Eulerian/Lagrangian framework have also successfully reproduced the features of the velocity field and scalar exchange within plant canopies (Ayotte *et al.*, 1999; Siqueira *et al.*, 2000; Katul *et al.*, 2001). The Lagrangian framework was chosen here because of the availability of measurements of velocity statistics within the canopy and to assess its aptitude for describing scalar transfer in a tall forest canopy.

The Lagrangian approach requires *a priori* specification of the wind field or turbulence statistics. In this analysis horizontal homogeneity is assumed and dispersion is considered only in the vertical. In this case, enough information to describe scalar transfer is given by the variance in vertical velocity σ_w^2 and the Lagrangian integral time scale T_L. The latter is a measure of the persistence of the turbulence and is generally not readily measured; rather a relationship to the Eulerian time scale is assumed, as discussed below.

In the localised near-field approach, the concentration of a scalar at a particular point is separated into near field and far field components:

$$C(z) = C_n(z) + C_f(z) \tag{2.1}$$

The near field component is related to the source strength through the probability that a fluid particle at initial position z_0 will be at position z at a later time t. This probability is encapsulated in the kernel function $k_n(\xi)$ for dimensionless position ξ.

$$C_n(z) = \int_0^\infty \frac{S(z_0)}{\sigma_{w0}} \left[k_n \left(\frac{z - z_0}{\sigma_{w0} T_{L0}} \right) + k_n \left(\frac{z + z_0}{\sigma_{w0} T_{L0}} \right) \right] dz_0 \tag{2.2}$$

where the integral is taken over all sources within the canopy and the kernel function is well approximated by $k_n(\xi) = -0.39894 \ln \left(1 - \mathrm{e}^{-|\xi|}\right) - 0.15623 \mathrm{e}^{-|\xi|}$ (Raupach, 1989a).

The far field component is given by:

$$C_f(z) = C(z_R) - C_n(z_R) + \int_z^{z_R} \frac{F(z)}{\sigma_w^2(z) T_L(z)} dz \tag{2.3}$$

where the integral is taken from z to a reference height above the canopy and $\sigma_w^2 T_L$ represents the far field turbulent diffusivity.

In the current study, velocity statistics were measured at four heights within the canopy and one above, and a third order polynomial was fitted to σ_w. The Lagrangian time scale has been estimated to scale roughly as $T_L \sim L_w/\sigma_w$ (Corrsin, 1963), where L_w is the Eulerian length scale for w. Near the top of the canopy L_w is of order $h/3$ (Raupach, 1988), where h is the height of the canopy top, and σ_w is typically around $1.1u_*$(Raupach, 1989b), where u_* is the friction velocity. T_L can therefore be expected to scale roughly with h/u_*. In this study T_L was assumed to follow the form:

$$T_L = a_2 \frac{1 - \exp(-a_1 z/h)}{1 - \exp(-a_1)} \frac{h}{u_*}$$

where a_1 and a_2 are parameters to be fitted. Depending on the optimal value found for a_1, the allowed forms for T_L within the canopy range from constant ($a_1 \to \infty$) to linear ($a_1 \to 0$), and are forced to zero at the ground. This covers the range of forms suggested for T_L from experimental results in the literature (Raupach, 1989b). From the above arguments the scaling factor a_2 is expected to be around 0.3.

2.1.2 Sun/shade leaf flux model

Previously the inverse Lagrangian approach has been implemented by dividing the canopy into a number of layers and finding the source strength in each layer from the measured concentration profile, utilising a discrete form of Equations (2.2) and (2.3) (see references in §1.5.1). In contrast, the present approach makes use of a sun/shade model to specify the continuous profile of source strength for the entire canopy layer. At a particular level

within the canopy, the source strength will be the leaf-level flux weighted by the leaf area index at that level. The CO_2, H_2O and sensible heat source strengths per unit canopy height are then obtained from:

$$S_c(z) = g_c\,(c_i - c_a)\,l \tag{2.4}$$

$$S_e(z) = g_e\,(e_i - e_a)\,l \tag{2.5}$$

$$S_H(z) = c_p g_H\,(\theta_l - \theta_a)\,l \tag{2.6}$$

where g_c, g_e and g_H are the conductances per unit projected leaf area (mol m^{-2} s^{-1}) for CO_2 and H_2O from the intercellular spaces to the canopy air space, and that for heat from the leaf surface to the canopy air space, respectively; c_i and c_a are the CO_2 concentrations (mol mol^{-1}) in the intercellular and canopy air spaces, respectively; e_i and e_a are the water vapour concentrations (mol mol^{-1}) in the intercellular and canopy air spaces, respectively; θ_l and θ_a are the potential temperatures (°C or K) of the leaf and canopy air, respectively (virtual potential temperatures are used when buoyancy effects are important); l is the leaf area index per unit height at height z (m^2 projected leaf area per m^3 air volume); and c_p (J mol^{-1} K^{-1}) is the molar specific heat capacity of air at constant pressure. The units of source strength are mol $m^{-3}s^{-1}$ for CO_2 and H_2O and W m^{-3} for heat.

The leaf area index profile was assumed to follow a beta distribution shown in Figure 2.1 and given by:

$$l\,(z) = \frac{\Lambda}{h} \frac{\frac{z}{h}^{(l_1-1)}\left(1-\frac{z}{h}\right)^{(l_2-1)}}{\int_0^1 t^{(l_1-1)}\,(1-t)^{(l_2-1)}\,dt} \tag{2.7}$$

where Λ is the total projected leaf area index (m^2 leaf area per m^2 ground area); h is the canopy height (m); t is a dummy variable; and the parameters $l_1 = 5$ and $l_2 = 4$ specify the width and height of the peak in leaf area. These parameters were chosen to give a leaf area distribution consistent with the observed height range of leaves within the canopy.

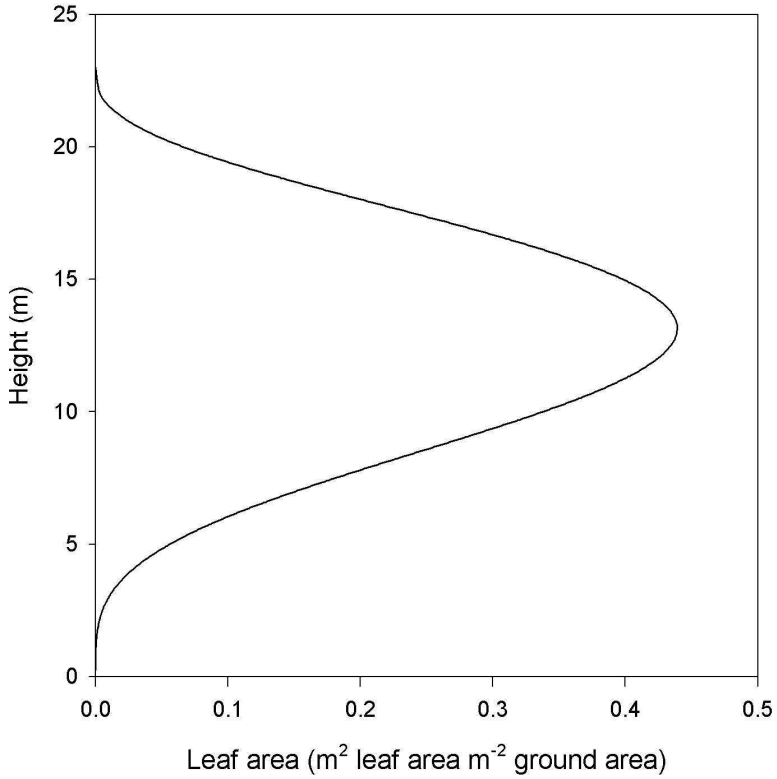

Figure 2.1: Assumed profile of leaf area within the canopy.

Cumulative leaf area from the top of the canopy was calculated from Equation (2.7) as:

$$\begin{aligned} L(z) &= \int_z^h l(z)dz \\ &= \Lambda - \int_0^z l(z)dz \\ &= \Lambda \left[1 - \frac{\int_0^{\frac{z}{h}} \frac{z}{h}^{(l_1-1)} (1-\frac{z}{h})^{(l_2-1)} dz/h}{\int_0^1 t^{(l_1-1)} (1-t)^{(l_2-1)} dt} \right] \end{aligned}$$

This can be calculated as the incomplete beta function $I_x(a,b)$ (see for example Press *et al.*, 1992), noting that $I_x(a,b) = 1 - I_{1-x}(b,a)$ and this function is defined as:

$$I_x(a,b) = \frac{\int_0^x t^{(a-1)}(1-t)^{(b-1)}dt}{\int_0^1 t^{(a-1)}\,(1-t)^{(b-1)}\,dt} \quad ,$$

resulting in the following expression for cumulative leaf area from the top of the canopy:

$$L(z) = \Lambda I_{1-z/h}(l_2, l_1)$$

Equations (2.4) to (2.6) sum the leaf-level fluxes over all leaves at a particular level (through the factor l) to give a "big leaf" flux per unit height for that level, here termed the source strength. To obtain the flux through a plane at height z in the absence of advection, the source strengths were integrated through all levels below, so that:

$$F(z) = F_g + \int_0^z \left(S(z') - \frac{dC(z')}{dt} \right) dz' \tag{2.8}$$

where F_g is the ground flux. Equation (2.8) neglects advection and applies to non-steady state conditions. Within the forest canopy CO_2 concentrations build up overnight due to respiration and usually low turbulence intensity, particularly close to the ground, and are depleted during the day. This provides a mechanism for a diurnal cycle in storage of CO_2 within the canopy, or time-dependence of CO_2 concentration, which is accounted for by the last term in the integral in Equation (2.8). The same applies to the other scalar quantities, to a lesser extent. In the model calculations time dependence was approximated by rate of change between hourly sampling periods, or three-hourly in the case of the isotope data.

Equation (2.8) combined with Equations (2.4) to (2.6) then leads to flux equations for CO_2, H_2O and heat. Three additional unknown parameters are introduced: the fluxes of these entities at the ground. These were determined through the optimisation procedure of the model.

Photosynthesis model

Leaf level carbon assimilation was modelled following de Pury and Farquhar (1997), based on the photosynthesis model of Farquhar *et al.* (1980). Leaves were separated into sunlit and shaded fractions with sunlit fraction declining exponentially with cumulative leaf area from the top of the canopy. Assimilation per unit leaf area at a particular level in the canopy was calculated for sun and shade leaves separately as the minimum of the Rubisco-limited and electron transport-limited rates:

$$A = \min\{A_V, A_J\} - R_l \tag{2.9}$$

where R_l is the leaf respiration per unit leaf area. The Rubisco-limited photosynthesis rate is given by:

$$A_V = \frac{V_l\,(c_i - \Gamma_*)}{c_i + K_c\left(1 + \frac{o}{K_o}\right)} \tag{2.10}$$

and the electron transport-limited photosynthesis rate is given by:

$$A_J = \frac{J\,(c_i - \Gamma_*)}{4\,(c_i + 2\Gamma_*)} \tag{2.11}$$

where c_i is the intercellular CO_2 concentration; Γ_* is the CO_2 compensation point in the absence of mitochondrial respiration; K_c and K_o are the Michaelis-Menten constants of Rubisco for CO_2 and O_2, respectively; o is the oxygen partial pressure in the intercellular spaces; V_l is the photosynthetic Rubisco capacity per unit leaf area; and J is the potential electron transport rate per unit leaf area. Except for J, variation of these parameters with temperature was determined using the temperature response functions reported by Bernacchi *et al.* (2001).

The response of electron transport to irradiance was determined from:

$$\theta J^2 - (I_l + J_m) J + I_l J_m = 0$$

where θ is the curvature of the response; I_l is the photosynthetically active radiation (PAR) effectively absorbed by photosystem II per unit leaf area, taken as 42.5% of total PAR absorbed by the leaf; and J_m is the maximum electron transport rate per unit leaf area. The ratio of J_m to V_l varies with temperature due to their different temperature response curves (Walcroft *et al.*, 1997; Leuning 1997). Here the ratio and temperature response curve for J_m of de Pury and Farquhar (1997) were used.

Photosynthetic capacity V_l was assumed to be linearly related to nitrogen content per unit leaf area. Since leaf nitrogen content did not vary appreciably with height in this canopy, it was assumed that V_l was approximately constant with height also. Leaf nitrogen was estimated as around 150 mmol m^{-2} from nitrogen determinations for fir and spruce leaves from the site up to two-thirds canopy height (see §2.2), and a typical proportionality constant between and leaf nitrogen found for coniferous species is around 0.2 at 20°C (Kellomäki and Wang, 2000a). It is expected that V_l will vary considerably for different species, climates and nutrient status. In particular, it has been argued that trees growing in boreal regions may take two to three months after snow melt to regain their maximum photosynthetic capacity (Bergh *et al.*, 1998). Therefore, as this study was undertaken not long after snow melt, in the absence of leaf-level gas exchange measurements during the study period V_l was left as a parameter to be fitted by the model.

Radiation penetration

Profiles of absorbed irradiance were calculated for sunlit and shaded leaves separately, following de Pury and Farquhar (1997). Shaded leaves receive diffuse and scattered beam irradiance while sunlit leaves additionally receive direct irradiance. The sunlit fraction was calculated as:

$$f_{sun} = \exp\left(-\frac{k_b}{\cos\phi_z}L\right) \tag{2.12}$$

where L is the cumulative leaf area from the top of the canopy; k_b is the beam radiation extinction coefficient; and ϕ_z is the solar zenith angle.

Absorbed diffuse PAR irradiance was calculated according to:

$$I_d = I_{d0}k'_d\left(1-\rho_{cd}\right)\exp\left(-k'_dL\right) \tag{2.13}$$

where I_{d0} is the diffuse PAR above the canopy; ρ_{cd} is the canopy reflection coefficient for diffuse PAR; and $k'_d = k_d\sqrt{1-\sigma_{\mathrm{PAR}}}$ is the diffuse PAR extinction coefficient incorporating the effect of scattering by leaves, where $\sigma_{\mathrm{PAR}} = 0.15$ is the scattering coefficient for PAR. Absorbed scattered beam irradiance was calculated as:

$$I_{bs} = I_{b0}\left[\left(1-\rho_{cb}\right)\frac{k'_b}{\cos\phi_z}\exp\left(-\frac{k'_b}{\cos\phi_z}L\right) - \left(1-\sigma_{\mathrm{PAR}}\right)\frac{k_b}{\cos\phi_z}\exp\left(-\frac{k_b}{\cos\phi_z}L\right)\right] \tag{2.14}$$

and absorbed beam radiation for sunlit leaves is given by:

$$I_b = I_{b0}\left(1-\sigma_{\mathrm{PAR}}\right)\frac{\overline{\cos\alpha_l}}{\cos\phi_z} \tag{2.15}$$

where I_{b0} is the beam PAR above the canopy; ρ_{cb} is the canopy reflection coefficient for direct PAR; $k'_b = k_b\sqrt{1-\sigma_{\mathrm{PAR}}}$ is the direct PAR extinction coefficient incorporating scattering; and $\overline{\cos\alpha_l}$ is the mean cosine of leaf angle. Leaves were divided into nine leaf angle classes and the mean cosine calculated for each class. The canopy reflection coefficients were calculated from the scattering coefficient as in de Pury and Farquhar (1997). Variation of scattering coefficient with leaf angle was neglected: any such variation should be small because while reflectance increases at glancing angles, this is offset by

a decrease in transmittance (Ross, 1981). In the calculation of extinction coefficients modified for scattering and canopy reflection coefficients the simplification is made that reflection and transmission coefficients are equal. This approximation has negligible effect when the reflection and transmission coefficients differ by less than 20%, and only a small effect otherwise (Goudriaan, 1977).

An additional minor contributing term accounts for reflection of direct beam radiation from the ground:

$$I_r = \sigma_S k'_d I_{b0} \exp\left(-\frac{k'_b L}{\cos\phi_z}\right) \exp\left[-k'_d\left(\Lambda - L\right)\right]$$

where σ_S is the surface reflectance. The relatively high value of 0.5 was assigned to σ_S because there was still a lot of (old) snow on the ground. Total irradiance received by sunlit leaves is then $I_{sun} = I_d + I_{bs} + I_r + I_b$, while shaded leaves receive $I_{shade} = I_d + I_{bs} + I_r$.

For random leaf orientation the leaf directions may be envisaged as evenly distributed over the surface of a sphere. The extinction coefficient for beam radiation k_b is then calculated to be 0.5, the ratio of the projected area of a hemisphere to its surface area (Cowan, 1968). A value for the diffuse radiation extinction coefficient k_d can be determined by integrating diffuse irradiance over the sky assuming a particular distribution of intensity (Cowan, 1968) and fitting an exponential curve to the solution (Goudriaan, 1977). The value thus found depends slightly on the leaf area index, but is around 0.78 (de Pury, 1995). Penetration of diffuse radiation is less than direct beam radiation except at low solar elevations because a large proportion of diffuse light emanates from the lower part of the sky. Factors that can lead to significant departures from these theoretical extinction coefficients include more regular leaf arrangements, leaf clumping and penumbral effects. The latter two factors are particularly important for coniferous forests. Kellomäki and Wang (2000b) determined a needle clumping factor from measurements of diffuse radiation in a Scots pine canopy, and obtained effective extinction coefficients for direct and diffuse

short wave radiation of 0.33 and 0.19, respectively. In the present study the two extinction coefficients k_b and k_d were determined by the optimisation procedure.

Conductances

The conductances to heat, H_2O and CO_2 are related to resistances by:

$$g_c = \frac{1}{r_{sc} + r_{bc}}$$

$$g_e = \frac{1}{r_{se} + r_{be}}$$

$$g_H = \frac{1}{r_{bH}}$$

where resistances to diffusion are denoted by r and are simply the inverse of conductance; r_{sc} and r_{se} are stomatal resistances to diffusion of CO_2 and H_2O from the intercellular spaces to the leaf surface; r_{bc}, r_{be} and r_{bH} are boundary layer resistances to diffusion of CO_2, H_2O and heat from the leaf surface to the canopy air space. Conductance for different entities through stomata are related by the ratio of their molecular diffusion coefficients (D_m) through air, so that $g_{se} : g_{sc} = 1.6 : 1.0$. Conductance through the leaf boundary layer is also by diffusion but the effective boundary layer thickness is dependent on D_m, being approximately proportional to $D_m^{\frac{1}{3}}$. Since conductance across a boundary layer is inversely proportional to the boundary layer thickness, the ratios here are then related by the $\frac{2}{3}$ power of the diffusion coefficients, $g_{bc} : g_{be} : g_{bH}/2 = 0.76 : 1.08 : 1.00$ (Jones, 1992). The factor of $\frac{1}{2}$ for g_{bH} accounts for the assumption of hypostomatous leaves, so that heat conductance occurs from both sides of the leaf, while CO_2 and H_2O are exchanged only on one side. Whether the leaves were truly hypostomatous is not critical because the stomatal conductance is essentially optimised (through λ, see below, and V_l), which compensates for any erroneous offset due to this assumption.

Stomatal conductance was modelled according to the theory of optimal stomatal behaviour (Cowan and Farquhar, 1977; Cowan, 1977). Using the argument that the carbon

gain through assimilation should be maximised for a given amount of water loss through transpiration over a daily time scale, the following form for stomatal conductance for CO_2 is found (see Appendix A for derivation):

$$g_{sc} = \frac{A}{\sqrt{\frac{1.6D_0}{\lambda}(c_a - \Gamma)} - 1.6\frac{A}{g^*_{be}}} \tag{2.16}$$

where $D_0 = D_a + \varepsilon r^*_{bH} R^*_{n,abs} \big/ \lambda_E$ is the leaf to air molar vapour concentration difference when the stomata are fully closed, with D_a the molar vapour concentration deficit of the air and $R^*_{n,abs}$ the absorbed isothermal net radiation (see leaf energy balance below); λ is the constant value of $\partial E/\partial A$; Γ is the CO_2 compensation point; and g^*_{be} is the effective boundary layer conductance to water vapour and heat loss: $g^*_{be} = \frac{1}{r_{be} + \varepsilon r^*_{bH}}$, where $r^*_{bH} = \frac{1}{g_{bH} + 4\varepsilon_l \sigma \theta_a^3 / c_p}$ is the effective boundary layer resistance to heat with ε_l the emissivity of the leaf surface and σ the Stefan-Boltzmann constant; and $\varepsilon = s\lambda_E/c_p$ is the ratio of the change in latent heat with temperature to the change in sensible heat, with s the slope of saturation vapour concentration with temperature. The second term in the denominator in Equation (2.16) results from expressing transpiration in terms of the vapour pressure deficit of the ambient air, accounting for the effect of heat transfer across the leaf boundary layer.

The constant λ in Equation (2.16), the marginal water loss per unit carbon gain, has been estimated as 250 mol mol^{-1} (moles of water lost per mole of carbon gained) for cool coniferous forests from a survey of gas exchange measurements (Lloyd and Farquhar, 1994). Arneth *et al.* (2002a) used eddy covariance measurements and modelled canopy conductance over a few days spread across the summer to infer $\lambda = 445$ mol mol^{-1} for a *Pinus sylvestris* forest in the vicinity of the present study site. For that same site and by a similar method Lloyd *et al.* (2002b) found values of 416 and 815 averaged over two different growing seasons. Hari *et al.* (1999) found $\lambda \approx 175$ also for *Pinus sylvestris* but at a site in Finland. Values worldwide over various other biomes range from 300 to 1500 (Lloyd and Farquhar, 1994). Since this parameter can greatly influence the relative rates

of transpiration and assimilation and has not been well characterised for the study site, it was left to be determined by the optimisation procedure.

Boundary layer conductance was assumed to be proportional to the square root of wind speed, with wind speed declining exponentially with normalised height from that at the canopy top, with extinction coefficient 3. This coefficient was chosen to fit wind speed measured within the canopy, and is consistent with other values reported for forests (1.7-3.2: Kaimal and Finnigan, 1994). Boundary layer conductance to heat transfer (from one side of the leaf) was then calculated as (Jones, 1992):

$$g_{bH} = \rho\sqrt{c_H \frac{u}{d}} \tag{2.17}$$

where the constant is taken as $c_H = 1.09 \times 10^{-5}$, with dimensions of a diffusion coefficient ($\mathrm{m^2 s^{-1}}$); u is the wind speed ($\mathrm{ms^{-1}}$); and d is a characteristic dimension of the leaf, taken as 0.001 m.

Solving for A, g_{sc} and c_i

The leaf-level CO_2 flux (Equation (2.4) without the factor l), stomatal conductance (Equation (2.16)) and boundary layer conductance (Equation (2.17) adjusted for CO_2) were solved simultaneously with Equation (2.10) or (2.11) for Rubisco-limited and electron transport-limited assimilation rates, respectively, as detailed in Appendix B.

Leaf energy balance

The water vapour concentration in the leaf intercellular air spaces must be close to the saturation vapour concentration at leaf temperature. This can be determined from the empirical relationship (Jones, 1992):

$$e_{sat}(\theta_l) = \frac{C_1}{P} \exp\left(\frac{C_2\theta_l}{C_3 + \theta_l}\right) \tag{2.18}$$

where θ_l is in °C; P is the atmospheric pressure (Pa); the constants are $C_1 = 613.75$, $C_2 = 17.502$, $C_3 = 240.97$; and $e_{sat}(\theta_l)$ is in mb.

Leaf temperature was obtained from energy budget considerations for each source level:

$$H + \lambda_E E = R^*_{n,abs} - \varepsilon_l \sigma \left(\theta_l^4 - \theta_a^4\right) \tag{2.19}$$

where H is the sensible heat flux; $\lambda_E E$ the latent heat flux; and $R^*_{n,abs} = dR^*_n/dL$ the isothermal net radiation absorbed; and all are expressed per unit projected leaf area at each source level. Isothermal net radiation is the net radiation that would result if the surface (leaves in this case) was at air temperature. Heat flux into stems was assumed to be negligible.

Leaf radiation balance was determined as the sum of PAR, near infra-red (NIR) and long wave (LW) contributions. Absorbed NIR was calculated for sun and shade leaves separately as for PAR (Equations (2.13)-(2.15)) but with scattering coefficient $\sigma_{\mathrm{NIR}} = 0.8$. Long wave radiation from the sky and ground were assumed to decline with cumulative leaf area from the top and bottom of the canopy, respectively, as for diffuse PAR, with scattering coefficient $\sigma_{\mathrm{LW}} = 0$. The extinction coefficient for LW radiation is just that for diffuse radiation, k_d, since it is emitted in all directions equally. Values before attenuation within the canopy were taken as measured downward LW radiation in the case of the sky, and black body radiation calculated for the ground assuming a temperature of 0°C, so that:

$$I_{LW,sky}\downarrow = I_{LW0}\downarrow \; k_d \exp(-k_d L)$$

$$I_{LW,ground}\uparrow = \varepsilon_g \sigma \theta_g^4 \exp[-k_d\,(\Lambda - L)]$$

Downward and upward LW radiation components from the surrounding canopy including emission from the level in question were determined for isothermal leaves as (see Appendix C for derivation):

$$I_{LW,canopy}\downarrow = \varepsilon_l \sigma \theta_a^4 \left[1 - \exp(-k_d L)\right]$$

$$I_{LW,canopy}\uparrow = \varepsilon_l \sigma \theta_a^4 \left\{1 - \exp\left[-k_d \left(\Lambda - L\right)\right]\right\}$$

where the extinction coefficient is again k_d. Reflected PAR and NIR were also included in the leaf radiation budget, assuming a ground reflectance of 0.5 for both.

The leaf flux equations for heat and water were then put into the energy budget and solved iteratively for leaf temperature:

$$\theta_l = \theta_a + \frac{R^*_{n,abs} r_e - \lambda_E D}{c_p \frac{r_e}{r_H} + 4\varepsilon_l \sigma \theta_a^3 r_e} \tag{2.20}$$

where D is the difference in specific humidity between the ambient air and the intercellular spaces, and the approximation $\left(\theta_l^4 - \theta_a^4\right) \approx 4\theta_a^3 \left(\theta_l - \theta_a\right)$ has been made. Iterations are necessary since D depends on leaf temperature (Equation (2.18)), though a good first approximation can be obtained by linearising e_i with respect to leaf and air temperature difference.

Isotopic discrimination

Further information on leaf-level carbon fluxes can be obtained from the isotopic composition of atmospheric CO_2 within and above the forest canopy. Isotopic fractionations associated with photosynthesis and respiration can be incorporated into the inverse analysis by consideration of the molar balance of the minor isotope (Raupach, 2001b).

Isotopic composition, denoted by δ, is reported with respect to an international reference material: $\delta = R_S/R_R - 1$, where R_S and R_R are the ratios of minor to major isotope abundance in the sample and reference material, respectively. The reference materials used here are PDB-CO_2 (CO_2 derived from the Pee-Dee Belemnite calcite formation) for

isotopic composition of CO_2 and SMOW (Standard Mean Ocean Water) for isotopic composition of H_2O. Isotope discrimination is denoted by Δ and is the deviation of the ratio of isotopic abundances in the ambient air and in the assimilation flux of CO_2 from unity: $\Delta = R_a/R_A - 1$, where R_a and R_A are the ratios of minor to major isotope abundance in atmospheric CO_2 and CO_2 assimilation flux, respectively. A positive discrimination during photosynthesis therefore leads to an increase in abundance of the minor isotope in the air.

Carbon isotopic discrimination during photosynthesis is related to intercellular CO_2 concentration by (Farquhar *et al.*, 1982):

$$\Delta^{13}\mathrm{C} = a + (b - a)\,\frac{c_i}{c_a} \tag{2.21}$$

where a is the fractionation occurring during diffusion through air (4.4‰) and b is that occurring during carboxylation (effective value taken to be 27‰). Taking into account also respiratory fluxes of CO_2 and their associated $^{13}C/^{12}C$ ratio within the ecosystem, measurements of carbon isotope composition of CO_2 within the canopy therefore help to constrain the leaf intercellular CO_2 concentration of the photosynthesising foliage. In the model scheme used here this simultaneously constrains stomatal conductance, transpiration and photosynthetic CO_2 assimilation rates. For a general discussion of these issues at the plant physiological level refer to Farquhar *et al.* (1989a).

Oxygen isotope discrimination was modelled in an analogous manner (Farquhar and Lloyd, 1993; Farquhar *et al.*, 1993):

$$\Delta^{18}\mathrm{O} = \bar{a} + \frac{c_c}{c_a - c_c}\,(\delta_c - \delta_a) \tag{2.22}$$

where $\bar{a}$ is the weighted average discrimination occurring during diffusion from the canopy air space to the sites of carboxylation (estimated as 7.4‰); c_c and c_a are the CO_2 concentrations in the chloroplast and ambient air, respectively; and δ_c and δ_a are the isotopic

compositions of CO_2 in the chloroplast and ambient air, respectively. In accordance with experimental evidence, a rough approximation to CO_2 concentration in the chloroplast was taken as that in the intercellular spaces less $0.1c_a$ (Farquhar and Lloyd, 1993; Evans and von Caemmerer, 1996).

CO_2 in the chloroplast is assumed to be in isotopic equilibrium with chloroplast water and isotopic exchange is catalysed by the enzyme carbonic anhydrase, with a fractionation factor of 41.2‰ at 25°C (O'Neill *et al.*, 1975). Isotopic composition of chloroplast water was modelled as for a free water surface (Craig and Gordon, 1965), with kinetic fractionation factor appropriate for the leaf boundary layer (Farquhar *et al.*, 1989b):

$$\delta_E = \delta_S + \varepsilon_k + \varepsilon^* + (\delta_V - \delta_S - \varepsilon_k)\,\frac{e_a}{e_i} \tag{2.23}$$

where δ_S is the oxygen isotopic composition of source water; δ_V is that of water vapour in the surrounding air; ε_k is the kinetic fractionation factor (28.5‰ through the stomata and 18.9‰ in the boundary layer, with the effective fractionation calculated from the relation $\varepsilon_k = \frac{28r_{se}+19r_{be}}{r_{se}+r_{be}}$, Farquhar *et al.*, 1989b); ε^* is the proportional depression of equilibrium vapour pressure by the heavier molecule (9.4‰ at 25°C, and temperature variation calculated from the relation $\ln\varepsilon^* = \frac{1137}{\theta^2} - \frac{0.4156}{\theta} - 2.0667 \times 10^{-3}$ with θ in K, Majoube, 1971); and e_a and e_i as before are the vapour pressures in the ambient air and intercellular spaces, respectively.

Equations (2.22) and (2.23) show that the oxygen isotope composition of CO_2 can also help to constrain both the assimilation and transpiration rates through its relationship with c_i and e_i.

The concentration and leaf-level flux of the minor isotope (denoted CO_2^* to represent either $^{13}CO_2$ or $C^{18}O^{16}O$) are related to those of the major isotope (CO_2) through the definition of Δ and modelled isotopic composition of canopy air:

$$\Delta = \frac{\left([CO_2^*] \,/\, [CO_2]\right)_a}{\left([CO_2^*] \,/\, [CO_2]\right)_A} - 1$$

where the subscripts a and A refer to the air and assimilation flux, respectively, which can be recast using the notation of Equation (2.4) as:

$$\Delta = \frac{c_a^*/c_a}{S_c^*/S_c} - 1 \tag{2.24}$$

where again the asterisk denotes the minor isotope. Hence, rearranging Equation (2.24), the leaf-level flux of the minor isotope is found from that of the major isotope and discrimination calculated from either Equation (2.21) or (2.22) as:

$$S_c^* = \frac{S_c R_a}{\Delta + 1}$$

2.2 Methods

2.2.1 Model inversion procedure

Using observations of concentrations of CO_2, $^{13}CO_2$, $C^{18}O^{16}O$, H_2O and temperature, the adjustable canopy and turbulence parameters and ground fluxes were optimised using a Levenberg-Marquardt procedure as described in Appendix D, minimising the difference between measured and modelled concentrations.

Input parameters for the photosynthesis model taken from the literature are given in Table 2.1, and measured input meteorological parameters are listed in Table 2.2. Carbon and oxygen isotopic composition of respired CO_2 were estimated as -26.0‰ and -16‰ (PDB-CO_2), respectively, from regression of isotopic composition with inverse CO_2 concentration (Keeling, 1961) using night-time flask data collected on the nights of 25, 27 and 29 May (Figures 2.2 and 2.3). Output model parameters were fitted using the hourly daytime periods which included concentrations of CO_2, $^{13}CO_2$, $C^{18}O^{16}O$, H_2O and temperature. There were five such periods on both 25 and 27 May for the hours beginning 06:00, 09:00, 12:00, 15:00 and 18:00 (local standard time) on each of the two days. Optimised values for ground fluxes of CO_2, H_2O and heat ($F_{C,g}$, $F_{E,g}$ and $F_{H,g}$), photosynthetic capacity (V_l), ratio of marginal water loss to marginal carbon gain (λ), extinction coefficient for

direct (k_b) and diffuse (k_d) radiation, and scaling constant (a_2) and extinction rate (a_1) of the Lagrangian time scale were obtained for each time period. Prior estimates were used for the canopy (V_l, λ, k_b and k_d) and Lagrangian time scale (a_1 and a_2) parameters in the optimisation and their ranges were restricted to lie within reasonable bounds. These bounds were: $V_l \geq 0.1$; $50 \leq \lambda \leq 1500$; $0 < k_b, k_d < 1$; $0.1 \leq a_1 \leq 100$; and $0.1 \leq a_2 \leq 0.6$. Prior estimates were obtained from the literature: $V_l = 45$ (the approximate value found by Kellomäki and Wang (2000a) for *Pinus sylvestris*); $\lambda = 250$ (Lloyd and Farquhar, 1994); $k_b = 0.5$ (spherical leaf angle distribution, Goudriaan, 1977); $k_d = 0.78$ (de Pury and Farquhar, 1997); $a_1 = 20$ and $a_2 = 0.3$ giving a T_L profile consistent with canopy data reviewed by Raupach (1989b). The level of constraint given by the prior estimates was dynamically adjusted to limit the parameters to the ranges given above when necessary.

Parameter	Value at 25°C and unit	Description
N_0	150 mmol m^{-2}	Leaf nitrogen content[1]
Γ_*	42.8 μmol mol^{-1}	CO_2 compensation point of photosynthesis in the absence of mitochondrial respiration[2]
J_m	$2.1V_l$	Electron transport rate per unit leaf area[3]
R_l	$0.0089V_l$	Leaf respiration rate per unit leaf area[3]
θ	0.7	Curvature of response of electron transport to irradiance[3]
K_c	405 μmol mol^{-1}	Michaelis-Menten constant of Rubisco for CO_2[2]
K_o	278 mmol mol^{-1}	Michaelis-Menten constant of Rubisco for O_2[2]
o	209 mmol mol^{-1}	Intercellular oxygen concentration

[1]Estimated from nitrogen content measurements; [2]Bernacchi *et al.* (2001); [3]de Pury and Farquhar (1997)

Table 2.1: Photosynthesis model input parameters

With these prior estimates the model was run for the ten profile sets containing $^{13}CO_2$ and $C^{18}O^{16}O$ data obtained on 25 and 27 May. The differences between modelled and measured concentrations were simultaneously minimised for all ten hourly periods to produce a single optimised canopy and turbulence parameter set (note that in contrast to this method, Styles *et al.* (2002b) used a weighted average of individual optimisations). Ground fluxes were optimised at the same time, but were not forced to be constant across the two days. The source code for the parameter optimisation is given in Appendix G,

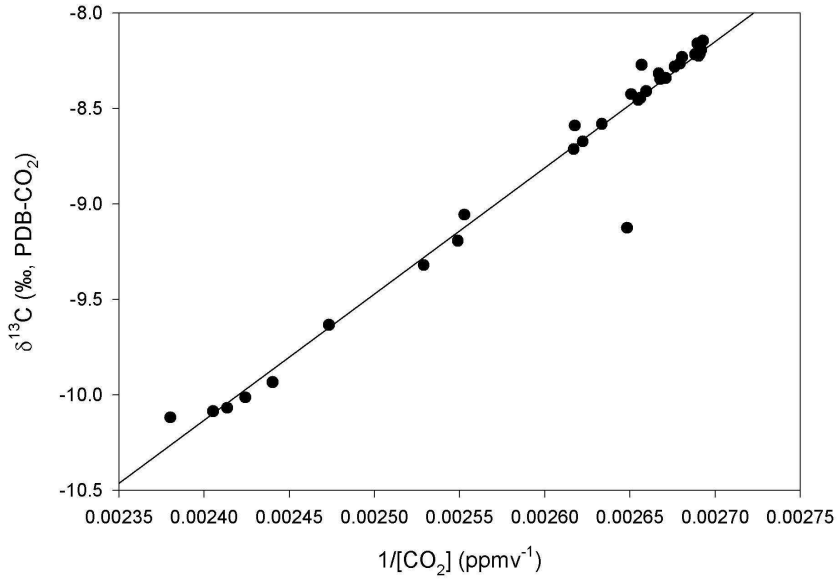

Figure 2.2: Carbon isotope composition versus inverse of CO_2 concentration for the nights of 25, 27 and 29 May, 2000. Linear regression through the data gave the equation $y = (6600 \pm 200)x - (26.0 \pm 0.5)$, $r^2 = 0.97$.

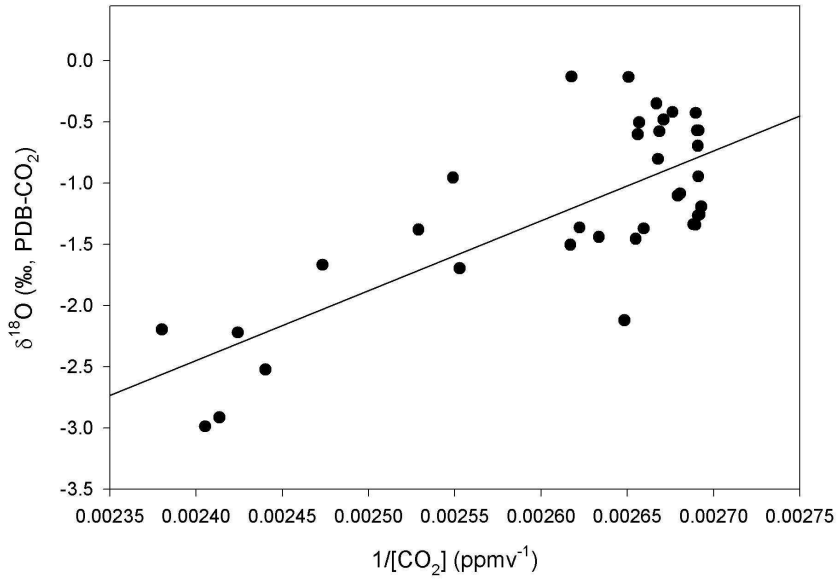

Figure 2.3: Oxygen isotope composition versus inverse of CO_2 concentration for the nights of 25, 27 and 29 May, 2000. Linear regression through the data gave the equation $y = (5700 \pm 800)x - (16 \pm 2)$, $r^2 = 0.57$.

Parameter	Description
$SWDR(z_R)$	Short wave downward radiation at reference height above the canopy
$LWDR(z_R)$	Long wave downward radiation at reference height above the canopy
$PAR(z_R)$	Incident photosynthetically active radiation at reference height above the canopy
f_D	Fraction of diffuse radiation above the canopy
$U(h)$	Wind speed at canopy top
u_*	Friction velocity
$\sigma_w(z)$	Standard deviation of vertical velocity within and above the canopy

Table 2.2: Measured meteorological input parameters

§G.1.1. Subroutines for calculating leaf level fluxes and turbulence characteristics are given in §G.2 in that Appendix.

The canopy and turbulence parameters were then fixed with these optimal values (given in Table 2.3) and the model was run over the ten-day period from 21 to 31 May for which hourly profiles of CO_2, H_2O and temperature were available, varying only the ground fluxes to fit the concentration data. Canopy fluxes were determined by integration of leaf level photosynthesis, transpiration and heat flux as described in §2.1 using above-canopy measurements of incident radiation, wind speed, CO_2 and H_2O concentrations and temperature, together with modelled within-canopy concentrations. The source code for the ground flux optimisation over the ten-day period is given in §G.1.2 in Appendix G.

2.2.2 Data collection

Site description

The field site was located at 62°N, 90°E, at an elevation of 160m, about 10 km east of the Yenisei River in central Siberia. The nearest settlement was the town of Zotino, about 30 km away on the west bank of the Yenisei River.

The forest consisted of a mix of mainly coniferous species: Siberian fir (*Abies siberica*, 59%), Siberian spruce (*Picea obovata*, 17%), Siberian pine (*Pinus siberica*, 6%), birch (*Betula pubescens*, ∼9%) and aspen (*Populus tremula*, ∼9%). The understorey included

Parameter	Value and unit	Description
$F_{C,g}$	*Variable*, μmol m^{-2}s^{-1}	Ground CO_2 flux
$F_{E,g}$	*Variable*, mmol m^{-2}s^{-1}	Ground H_2O flux
$F_{H,g}$	*Variable*, W m^{-2}	Ground sensible heat flux
V_l	26 μmol m^{-2}s^{-1}	Maximum photosynthetic Rubisco capacity
λ	130 mol mol^{-1}	Marginal water loss to carbon gain constant
k_b	0.37	Extinction coefficient for direct radiation
k_d	0.20	Extinction coefficient for diffuse radiation
a_1	23	Lagrangian time scale extinction coefficient within canopy
a_2	0.25	Lagrangian time scale ratio with h/u_* at canopy top

Table 2.3: Modelled output parameters

mosses, ferns, herbs and occasional shrubs. Tree density was about 1770 trees per hectare (trees with circumference >10cm at breast height). Canopy height was around 23m. Projected leaf area index was measured as 4.3±0.5 with a LAI-2000 (LICOR, Lincoln NE, USA). This value includes a correction for mutual shading of needles in coniferous forests as described by Gower and Norman (1991), the factor used here being their measured needle-area to shoot-silhouette-area ratio for Norway spruce of 1.6.

Sampling isotopes of CO_2

Flask samples were taken every three hours over three separate sampling periods during May 2000: 06:00 on 25 May to 01:00 on 26 May (7 profiles), 06:00 to 22:00 on 27 May (6 profiles) and 21:00 on 29 May to 04:00 on 30 May (3 profiles). Samples were collected at six heights: 0.4, 1.9, 10.1, 18.3, 22.2 and 29.3 metres with occasional missing data due to problems with the flask sampling units. Sampling lines were flushed for at least five minutes prior to sampling. Air was pumped at about 7 l min^{-1} through 5 mm Dekabon tubing from each sampling height to the ground. The sample line was connected to a large diameter (∼30mm) magnesium perchlorate trap to remove water vapour and minimise exchange of oxygen isotopes, and the flow then passed through a mass flow controller at 33 ml/min to fill an evacuated 1 litre flask to 2 atm (200 kPa) over one hour, with excess

air being vented. Just upstream of the flask was a $\frac{1}{16}''$ capillary placed as a pneumatic resistance to prevent fractionation during the first surge of air into the evacuated flask. Figure 2.4 shows a schematic representation of the flask sampling system. All parts downstream of the mass flow controller were of stainless steel to minimise isotopic exchange and adsorption of reactive species onto the walls. Flasks underwent a heating and flushing preconditioning treatment prior to use, carried out in the Institute for Environmental Physics in Heidelberg.

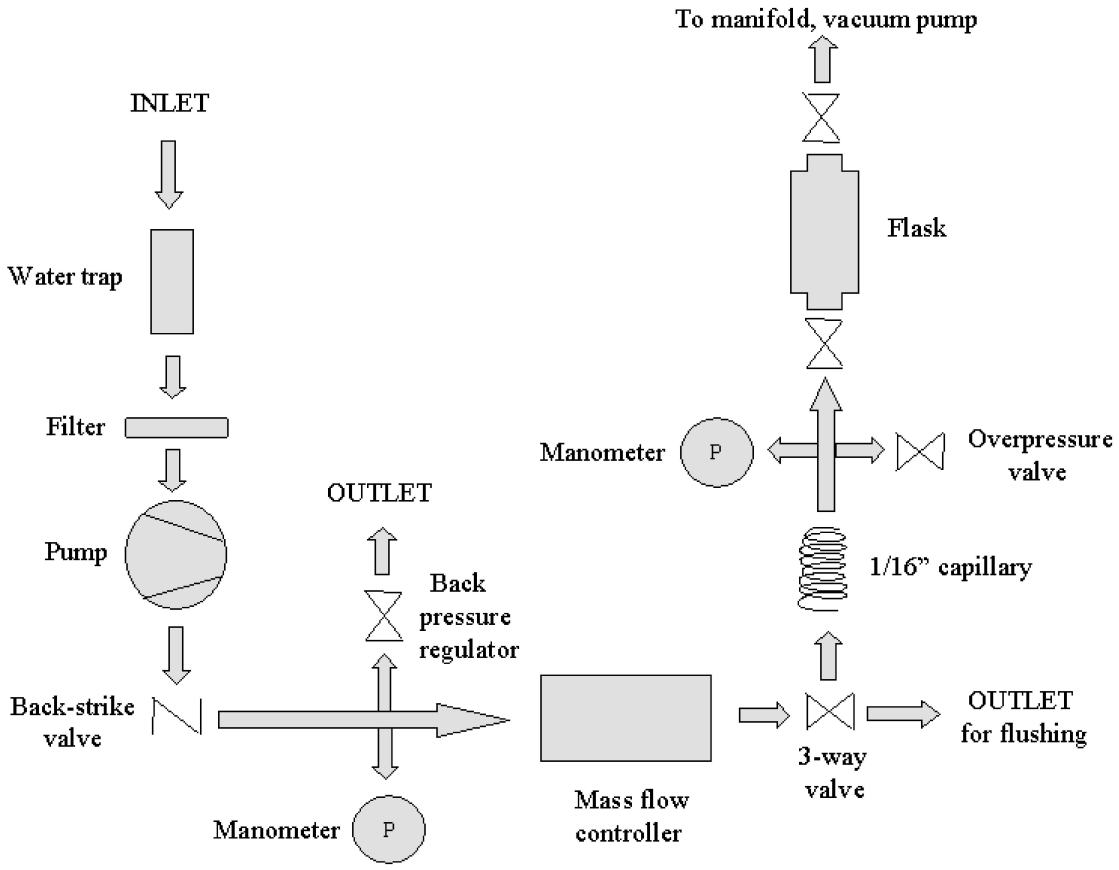

Figure 2.4: Schematic diagram of flask sampling system.

Sampling isotopes of precipitation, soil water and water vapour

Precipitation was collected from a tipping bucket rain gauge (model 52203, Young Instruments, Traverse City, MI, USA) and stored in 10 ml teflon vials sealed with PVC tape or Parafilm. The soil was fully saturated during the measurement period so soil water was

collected by drilling holes about 30 cm deep and collecting the water that immediately filled these holes in 10 ml teflon vials.

Water vapour samples were collected at four heights for analysis of oxygen and hydrogen isotopic composition. Air was drawn through teflon tubing from 2m, 18m, 22m and 28m heights at 150 ml min^{-1}. The air was passed through a 200mm glass column (diameter 15mm) immersed in ethanol cooled to -90°C with liquid nitrogen. An internal tube within the glass column ensured that the air passed to the bottom of the column before being vented. Tests with a second column in line showed that no measurable amount of water vapour escaped condensation. Vapour was collected in this manner over a four-hour period on 25 and 27 May from 12:00 to 16:00 in order to obtain enough liquid for storage and analysis. Liquid water was transferred to 10 or 25 μl capillaries via a syringe and sealed with sealing wax for transportation.

Concentration measurements

Concentrations of CO_2 and H_2O were measured continuously from May 18 to 30 with a LICOR 6262 infra red gas analyser (IRGA) sampling each of nine heights for one minute in every ten. Measurements were made at 0.1, 0.9, 2.2, 6.0, 10.1, 14.1, 18.3, 22.2 and 29.3 metres. The instrument was operated in absolute mode and was calibrated with gas of known CO_2 concentration and a dewpoint generator once a week. Hourly averages were obtained from the data logger record.

For the same period, temperature was measured at six heights with model 107 Temperature Probe thermistors (Campbell Scientific, Shepshed, Leicestershire, UK) installed with ventilated radiation shields. Measurement heights were 0.2, 2.1, 10.0, 18.4, 22.1 and 28.0 metres. Hourly averages were obtained from the ten-minute averages stored on the data logger for the period May 18 to 30.

Tower measurements

Downward and upward components of short and long wave radiation were measured above the canopy with a pyrradiometer (model LXG055, Dr Lange, Berlin, Germany) and

albedometer (model CM14, Kipp and Zonen, Delft, Netherlands). Also measured above the canopy were photosynthetic photon flux density (PPFD, model LI-190SA, LICOR, Lincoln, NB, USA), wind speed (model A100R, Vector Instruments, Rhyl, UK) and air pressure (model PTB101B, Vaisala, Helsinki, Finland). Net radiation was measured at two separate locations below the canopy with two net pyrradiometers (Middleton CN1-R, Melbourne, Australia). Diffuse downward radiation was measured at a separate study site about 40 km away using a pyranometer with regularly adjusted shadow ring (model CM11, Kipp and Zonen, Delft, Netherlands). Excellent agreement between the two sites for both downward short wave radiation and PPFD (slope=1.00, r^2=0.90) allowed extrapolation of the diffuse downward radiation measurements to the present study site.

Velocity statistics were measured at five heights with one sonic anemometer (model Solent R3, Gill Instruments, Lymington, Hampshire, UK) fixed above the canopy at 29.6 metres and another roving sonic at 2.0, 9.8, 15.8 and 21.8 metres. Eddy covariance measurements of carbon dioxide, water vapour and heat fluxes were made with an IRGA (LICOR 6262) and sonic anemometer above the canopy. The two IRGAs were located at the ground and air was pumped from the inlets at each height on the tower through 5mm internal diameter tubing at around 7 l min^{-1}. Details of the meteorological and eddy covariance measurements are described elsewhere (Röser *et al.*, 2002).

Leaf sampling

Needle samples were collected from two trees, one fir and one spruce, at 2-metre height intervals up to about half canopy height. Shoots were collected from several aspects of each tree, and needles collected randomly from each shoot to represent all needle-age classes and aspects, weighted roughly according to abundance. Needle widths and lengths were measured on a subset of these samples, and samples were sun-dried in paper bags before transportation for nitrogen analysis.

2.2.3 Instrument calibrations and corrections

Calibration of IRGAs

The profile and flux IRGAs were calibrated weekly using a dewpoint generator to provide known water vapour concentration and an air cylinder of approximately known CO_2 concentration. Zero was set using a cylinder of nitrogen gas. Later comparison with flask samples showed that the IRGA CO_2 concentration was underestimated by nearly 10 ppm in a consistent manner. This most likely reflects very poor accuracy in determination of the reference cylinder concentration, and a correction was applied to all IRGA CO_2 data to reflect the average offset of flask samples, 9.8±0.4 ppm (where the error estimate is the standard deviation of offset over all data). It is worth noting that in the canopy inverse analysis it is the deviation of concentrations from their value at the reference height that is important, so that this offset between the IRGA and flask data makes no difference to the calculations. Comparability of profile measurements of CO_2 and H_2O in terms of absolute accuracy was ensured by using a single instrument switching between heights.

The inlets of the tubing leading to the IRGAs were attached to small, downward-facing funnels to prevent liquid water entering by capillary action. The funnels were covered in fine, insect-proof gauze. The inlets were inspected weekly for condensation and insect invasion, but were always found to be clean during the measurement period.

Calibration of temperature sensors

Temperature probes were buried together under the snow for a period of several hours to determine their comparability. This test showed that two temperature probes which had extension leads disagreed significantly with the remaining four. This is because the measurements are sensitive to the extra resistance introduced by extending the cable, particularly if the extension cable is of poor quality. The extensions were removed and the datalogger relocated slightly to accommodate the shorter original cable lengths. Agreement between probes was then within 0.2°C, less than the accuracy given in the probe specifications (±0.4°C over the temperature range -20°C to +48°C). Consistent offsets

between the six probes were removed, corrected to the probe to be installed at the reference height above the canopy. These corrections were, from the 0.4m probe to the 22m probe in ascending order, in °C and with standard deviations of the offset as measured over a two-hour period given in brackets: +0.053 (0.006), -0.060 (0.010), +0.127 (0.006), +0.093 (0.006), +0.113 (0.006). These offsets directly affect the model calculations but their consistency and low magnitude suggest this is not a significant source of error in the model.

Calibration of radiometers

The two net radiometers to be positioned under the canopy were first fitted at the top of the tower with the above-canopy pyrradiometer for two days. The comparison showed that the top sensor overestimated net radiation by about 20% compared to the two ground radiometers. The deviant sensor was recalibrated after the measurement campaign and the above-canopy radiation data were corrected to the new calibration parameters, bringing this sensor into agreement with the ground radiometers over the two day comparison period. Recalibration of one of the ground radiometers after the experiment showed little difference with the prior calibration parameters.

Eddy covariance corrections

A number of steps were involved in the post-acquisition processing of eddy covariance data. Corrections and flux calculations were carried out using software developed by Olaf Kolle (Max Planck Institute for Biogeochemistry, Jena, Germany). The major corrections are described briefly here, with a more detailed description given in Röser *et al.* (2002).

The IRGA CO_2 and H_2O concentration measurements lagged the sonic anemometer velocity measurements by around 6 seconds due to travel time from the top of the tower to the instrument station at the ground. Accurate estimates of these lags were obtained by examination of cross correlation between the time series for vertical air velocity and each of those for CO_2 and H_2O. The latter series were then shifted by these lags before calculation of fluxes.

Dampening of high frequency fluctuations in concentrations due to mixing within the tubing while being drawn down to the IRGA at the ground and due to response time of the IRGA were corrected as described by Eugster and Senn (1995). The correction was determined by comparison of frequency cospectra of vertical velocity and temperature (both measured by the sonic anemometer) with those for vertical velocity and either CO_2 or water vapour. Coordinate rotation was applied as described in McMillan (1988) to correct for non-zero mean vertical velocity.

Interpolations

Concentration data were interpolated using the Akima cubic spline interpolation routine (IMSL Math Library, Visual Numerics) which minimises generation of artificial maxima and minima, to give continuous profiles from the lowest measurement height within the canopy to the reference height above the canopy. This was to simplify model calculations by providing concentration measurements for each scalar species at any source level being calculated. Caution must be taken when using interpolated values, however, since vertically adjacent "measurements" then become highly correlated, violating the assumption of independence implicit in the model optimisation approach (Press *et al.*, 1992). This problem was overcome by attaching larger measurement error to those interpolated values between measurements so as to give them little weight compared to those values near the actual measurements (this is in contrast to the study of Styles *et al.*, 2002, which gave equal weight to all interpolations).

2.2.4 Laboratory analyses

Isotopic composition of CO_2

Flask samples of air were analysed at the Max Planck Institute for Biogeochemistry in Jena for carbon and oxygen isotopic composition, $\delta^{13}C$ and $\delta^{18}O$, using a dual-inlet Finnigan MAT252 mass spectrometer. Analysis precision was estimated as 0.010 for $\delta^{13}C$ and 0.015 for $\delta^{18}O$. Aspects of the isotopic analysis procedure are discussed in Werner and Brand (2001).

Atmospheric concentration of CO_2, CO, N_2O, CH_4 and H_2

Flask samples were analysed for concentrations of CO_2, CO, N_2O, CH_4 and H_2 at the Max Planck Institute for Biogeochemistry using a double gas chromatograph system as described in Jordan and Brand (2001), with an estimated analysis precision of 0.08 ppm. The flask CO_2 measurements were used to correct the absolute scale of the IRGA CO_2 measurements as described above. Concentrations of other species determined for the flask samples were not used in this analysis and are not reported here.

Oxygen isotopic composition of water

Water samples were analysed for oxygen isotopic composition at the Research School of Biological Sciences, Australian National University, Canberra, by the method of Farquhar *et al.* (1997). 1 μl samples were transferred by pipette to tin capsules and hermetically sealed. Samples were pyrolysed at 1050°C for quantitative conversion of oxygen to carbon monoxide, then passed through a gas chromatograph for separation of CO from N_2 using a helium carrier flow in an elemental analyser (NA1500, Carlo Erba Strumentazione, Milan, Italy). Samples passed directly to a continuous flow isotope ratio mass spectrometer (Isochrom-EA, Micromass, Manchester, UK) where oxygen isotope composition was measured with respect to a reference CO gas. Absolute sample composition was obtained by correction to a range of water isotopic standards (ANU-C1, ANU-P1, GISP and SLAP, obtained from the Research School of Earth Sciences, Australian National University, Canberra and CSIRO Land and Water, Canberra) analysed in the same manner before and after a set of approximately ten sample runs.

Leaf nitrogen content

Dried needles were ground and analysed for nitrogen content at the Research School of Biological Sciences, Australian National University, Canberra. Samples of ~2 mg were combusted and passed through a gas chromatograph to separate CO_2 from N_2 in an elemental analyser (EA1108, Carlo Erba Strumentazione, Milan, Italy). Peaks were monitored with

a thermal conductivity detector and calibration of nitrogen content was obtained using nitrogen elemental standards.

2.3 Results

Modelled ecosystem (canopy plus ground) fluxes are compared with hourly-averaged eddy covariance flux measurements over the full ten day period in Figure 2.5. Also shown are the ground fluxes as fitted by the inversion procedure. This figure shows that the model was able to successfully predict the diurnal pattern of ecosystem CO_2 fluxes over many days, despite no information on the measured magnitude or overall pattern of the measured fluxes entering the fitting procedure.

The model also predicted reasonable patterns of ecosystem H_2O fluxes, though with some significant departures. Generally speaking, the model partitioned a significant portion of the total evaporation to the soil surface, but the inferred contribution of ground evaporation to the overall evaporation flux varied substantially from day to day (Figure 2.5b). The extreme departures from reasonable values correspond to periods during and following rain, where the model fails to account for wetting of leaf and soil surfaces and subsequent evaporation.

Similarly, the model reasonably predicted both the diurnal pattern and the overall magnitude of sensible heat fluxes (Figure 2.5c). The model found that during the day, the magnitude of the heat flux from the ground was generally much smaller than that from the canopy itself and usually negative in sign. As for the water vapour fluxes, sensible heat fluxes in periods during and following rain were poorly modelled.

The correlation between measured and modelled fluxes as determined by linear regression is shown in Figure 2.6. Data that were deemed to be affected by rain were excluded from the regression analysis, but are shown on the plots. These points were generally the periods up to about three hours after rainfall. This figure shows that there is a degree of scatter for CO_2, H_2O and sensible heat fluxes about the 1:1 line which likely reflects both the inability of the model to perfectly represent all environmental conditions, as well